that induced regionwide flash-flooding including a high flow event in the New Haven River (171 m^3/s; 6,040 cfs). Additional, smaller magnitude flow events that occurred during the study period could also be assumed to result in continued, minor erosion and sediment transport.

Table 1. Summary of survey characteristics and river level at time of survey

Survey Date	Survey Method	DEM Resolution (m)	Dowsnstream USGS River Stage (m)
Nov-2012	ALS	1.0	--
27-Apr-2016	eBee RTK UAS	0.15	1.12
18-Apr-2017	eBee Plus UAS	0.15	1.31
13-Apr-2018	eBee RTK UAS	0.15	1.45

METHODS

Topographic surveys: The 1.2 km New Haven River study site was surveyed using a fixed-wing eBee (SenseFly) UAS with an RGB true-color camera (Figure 1b). Three UAS surveys took place during a 2-yr period between spring 2016 and spring 2018 and were conducted in late April, prior to leaf-out (Table 1). River levels at survey time were generally low and varied by 0.33 m or less (based on downstream USGS river stage). Two eBee models were used in this study, the eBee RTK and eBee Plus. Both models feature a survey-grade system that uses a more accurate GPS receiver capable of using a virtual or local GPS base station, and therefore can eliminate the need for ground control points (GCPs). The virtual GPS base station was utilized to georeference the eBee RTK, which has a nominal accuracy of 5 cm. The data were collected at a target ground image resolution of 3.6 cm or finer with an overlap of 80% parallel and 60% perpendicular. Topographic data previously collected with an airborne laser scanning (ALS) survey were also used to calculate longer-term amounts of erosion along the study site. The existing ALS survey was collected in November 2012 at an average point spacing of 1.6 m.

DEM and DoD Analysis: The UAS imagery were first post-processed using senseFly's eMotion Version 3.3.4 software and then passed through the Pix4D Version 4.0.21 (Pix4D, Inc.) software package for photogrammetric processing. The latter provides a seamless workflow that utilizes UAS imagery and position information to generate a three-dimensional point cloud and derivative products including an orthorectified image mosaic, raster digital surface model, and raster DEM. Pix4D generates "bare-earth" DEMs using a proprietary, machine learning-based algorithm. The UAS-based DEMs had a cell size of 0.15 m compared to 1.0 m for the 2012 ALS.

DEM accuracies were evaluated using ground control points (GCPs) distributed within the river corridor area. The GCPs were surveyed using a TopCon HiperLite+ differential GNSS (Global Navigation Satellite System) receiver. A root mean square error (RMSE) was calculated in each direction (X, Y, Z) using the GCPs for each survey. To compare DEMs from multiple survey dates, DEMs of difference (DoDs) were generated in Quick Terrain Modeler Version 8.0.4 (Applied Imagery). The DoDs were calculated between successive UAS surveys as well as between UAS DEMs and the ALS DEM. The later survey date was always subtracted from the earlier date to compute DoD; thus, resulting negative values indicate erosion. Total erosion over the 20.3 ha (50.1 ac) vulnerable river corridor area (delineated area, Figure 2a and b) was calculated as the sum of the volume of the DoD below a reference zero plane. A total deposition volume was similarly calculated as well as the difference between total erosion and deposition providing a net volumetric change.

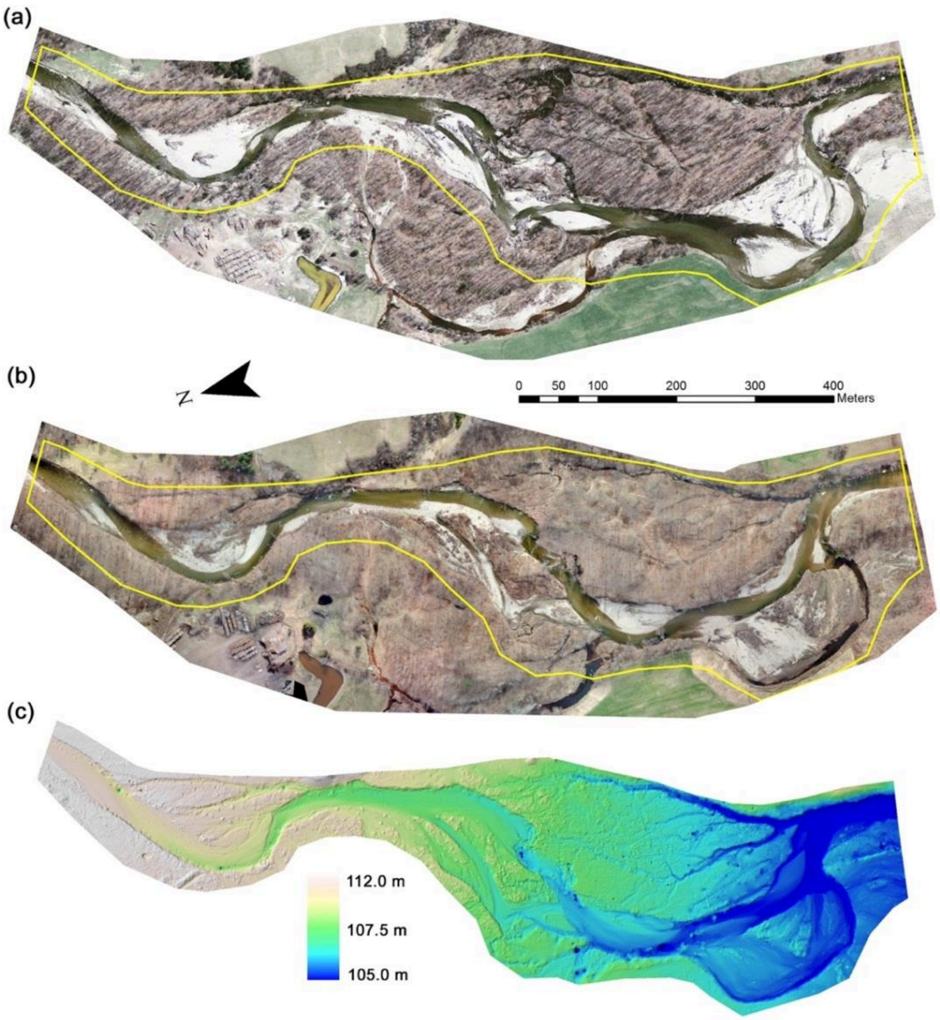

Figure 2. Section of the New Haven River as seen in (a) April 2012 aerial and (b) April 2018 UAS orthomosaic imagery. The yellow boundary represents area used in the DEM analysis. Elevation of "bare-earth" surface as shown in (c) DEM of 2018 UAS survey.

RESULTS AND DISCUSSION

UAS-derived Topographic Data: UAS surveys were successfully completed during early-spring, leaf-off conditions when ground surface visibility is highest (as evident in UAS imagery, Figure 2b). The "bare-earth" ground surface was also reliably represented in the DEMs automated using the Pix4D processing worklfow. For the April 2018 UAS survey, GCP positions in UAS data compared well to RTK-GPS surveyed GCP locations with low RMSE values of 0.04 m and 0.06 m in northing and easting, respectively, and 0.04 m in elevation. This compares well to the accuracy of the 2016 and 2017 UAS surveys as well as the 2012 ALS survey – previously analyzed by Hamshaw et al. (2018). As evident in the small error measures and lack of visual artifacts (i.e. excessive interpolation) in the UAS-derived DEMs (Figure 2c), the automated processes in Pix4D software for removing effects of vegetation are efficient and robust, even along the study river corridor which features varied vegetation and topography.

Bank Erosion and Change Detection: Bank failures along the 1.2 km New Haven River study area were common and occurred between each sequential surveys. Visual observations of bank failures at time of the spring 2016 and spring 2018 surveys suggest failure mechanisms likely include a combination of bank toe material removal and undercutting followed by geotechnical failure of the cantilevered overhang (see examples in Figure 1c and d). Noticeable deposition also occurred over the study period, primarily on inside river bends opposite eroding banks. The DoD analysis showed widespread geomorphic change between sequential surveys.

Over the six-year period between the 2012 ALS survey and 2018 UAS survey, the river corridor experienced a 14,050 m^3 net loss of material with a total erosion of 33,245 m^3 and total deposition of 19,193 m^3. A similar pattern of net material loss was observed between the intermediate (2016 and 2017) UAS surveys (Figure 3). However, between the 2017 and 2018 surveys, a large depositional volume (17,140 m^3) was observed resulting in a net aggradation (4,763 m^3) of material between 2017 and 2018. For erosion, 2016-2017 and 2017-2018 volumes were similar with 11,369 m^3 and 12,377 m^3 of bank material eroded, respectively. Of note, both erosion and deposition, the summed volumes for the intermediate 2012-2016, 2016-2017, and 2017-2018 periods were greater than volumes calculated between the first and last survey (2012-2018). Based on visual analysis of ortho-imagery and shifting patterns of erosion and deposition in DoDs (Figure 4), it is likely that intra-reach reworking of material is occurring, where areas initially subject to deposition are subsequently eroded, and vice-versa.

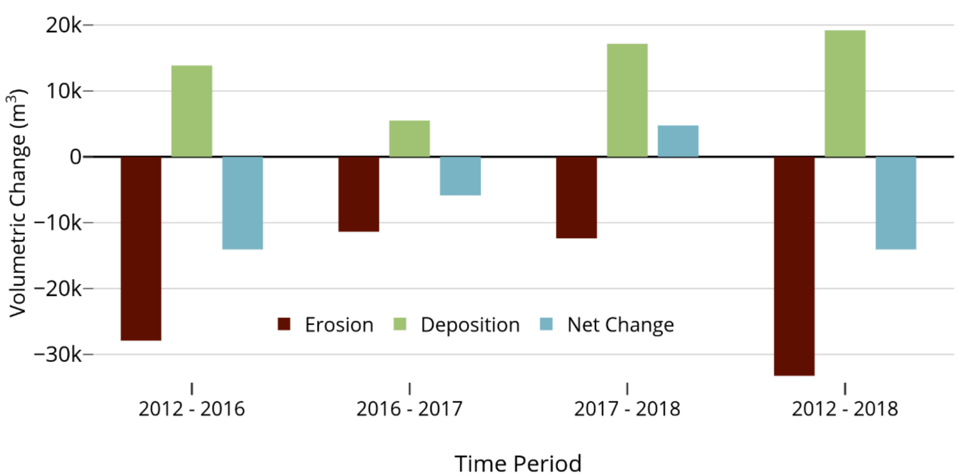

Figure 3. Volumetric change of river corridor area between surveys

Monitoring of Geomorphic Change: Use of consecutive DoD maps revealed spatial patterns of erosion and deposition at a fine scale in addition to providing the volumetric estimates of erosion and deposition. In both the 2012-2018 DoD (Figure 4a) and 2017-2018 DoD (Figure 4b), bank erosion is apparent along the outside of the meander bends with corresponding deposition on point bars located on the inside of the bend suggesting lateral accretion processes are occuring. The combination of multiple-year DoDs (e.g. 2012-2018 in Figure 4a) and single-year DoD (e.g. 2017-2018 in Figure 4b) allow for effective monitoring of geomorphic change at an annual scale (e.g., streambank failures) in the context of a longer-term, multi-year trends (e.g., a trajectory of reach-scale change, such as net aggradation or planform change) as the river responds to restoration efforts.

Limitations and Recommendations. The use of photogrammetric methods to capture topographic data along river corridors can be challenging due to the presence of varied vegetation and the possibility for erosion or deposition processes occurring below the water surface that are not well captured. Photogrammetric methods can be problematic in densely vegetated areas resulting in poor representation of a "bare-earth" surface (Hamshaw et al., 2017). In this study, errors due to dense vegetation were only recognizable in very limited areas. This was likely due to the survey being performed at the optimal time of the year (prior to vegetation growth). In areas with very dense vegetation or with year-round foliage, use of UAS-based photogrammetry may not be as effective. UAS-based photogrammetry has been shown capable of collecting bathymetric data; however, it is most effective with error correction due to refraction (Dietrich 2017, Woodget et al., 2015). In this study, error correction was not performed on the UAS data as the analysis focused on bank erosion and deposition. This may be a potential source of error in volumetric calculations, especially if large differences in river level were present across studies. Ideally, surveys should be collected at consistent, low water levels or evaluated by excluding below-water areas from analyses. In this project, the timing of surveys were selected to balance optimal vegetation conditions (early spring, prior to leaf-out) and consistent, reasonably low water levels (Table 1).

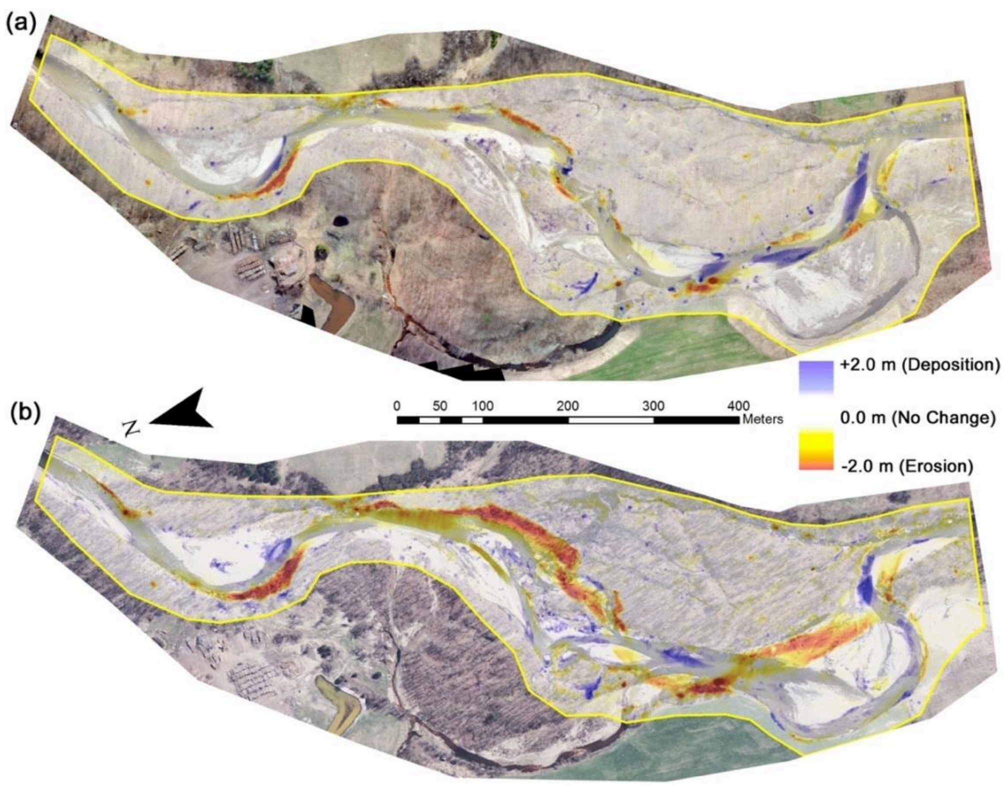

Figure 4. Elevation change between surveys as visualized by DEMs of difference (DoDs) between (a) 2017 UAS survey and 2018 UAS survey projected over 2018 imagery and (b) 2012 ALS survey and 2018 UAS survey projected over 2012 imagery.

CONCLUDING REMARKS

This case study focused on the monitoring of geomorphic change, specifically bank erosion and deposition, along a portion of the New Haven River and highlighted the utility of UAS photogrammetry for collecting fine-scale topographic data. UAS-derived topography was found to be similar in accuracy to existing airborne lidar survey and sufficient for reliable estimation of the magnitude of bank erosion and deposition. This allowed for the quantification of ongoing bank erosion and deposition as the river reach continuous to respond to restoration efforts. Limitations of the UAS methods can be addressed by conducting surveys during times of the year where vegetative growth is minimal, and by choosing survey dates with consistent river water levels that are as low as possible during those minimal-vegetation months. For projects with challenging site conditions and access such as those along river corridors, UAS-based photogrammetry provides a cost-effective and reliable method to inform project developement and provide ongoing monitoring for geomorphic change.

ACKNOWLEDGEMENTS

This research was supported by the Vermont Water Resources and Lakes Studies Center with additional support by Vermont EPSCoR with funds from the National Science Foundation (NSF) Grant EPS-1101317 and OIA-1556770, NSF Graduate Research Fellowship under Grant DGE-0925179NSF, the Robert & Patricia Switzer Foundation, the Gund Institute for Environment, and the US Department of Transportation (Grant OASRTRS-14-H-UVM). We also acknowledge additional contributions of the University of Vermont (UVM) Spatial Analysis Lab UAS team.

REFERENCES

Cavalli, M., Goldin, B., Comiti, F., Brardinoni, F., and Marchi, L. (2017). "Assessment of erosion and deposition in steep mountain basins by differencing sequential digital terrain models." *Geomorphology*, Sediment Dynamics In Alpine Basins, 291, 4–16.

Cook, K. L. (2017). "An evaluation of the effectiveness of low-cost UAVs and structure from motion for geomorphic change detection." *Geomorphology*, 278, 195–208.

Daly, E. R., Miller, R. B., and Fox, G. A. (2015). "Modeling streambank erosion and failure along protected and unprotected composite streambanks." *Advances in Water Resources*, 81, 114–127.

De Rose, R. C., and Basher, L. R. (2011). "Measurement of river bank and cliff erosion from sequential LIDAR and historical aerial photography." *Geomorphology*, 126(1–2), 132–147.

Dietrich, J. T. (2017). "Bathymetric Structure-from-Motion: extracting shallow stream bathymetry from multi-view stereo photogrammetry." *Earth Surface Processes and Landforms*, 42(2), 355–364.

Eltner, A., Kaiser, A., Abellan, A., and Schindewolf, M. (2017). "Time lapse structure from motion photogrammetry for continuous geomorphic monitoring." *Earth Surface Processes and Landforms*.

Fonstad, M. A., and Marcus, W. A. (2010). "High resolution, basin extent observations and implications for understanding river form and process." *Earth Surface Processes and Landforms*, 35(6), 680–698.

Hamshaw, S. D., Bryce, T., Rizzo, D. M., O'Neil-Dunne, J., Frolik, J., and Dewoolkar, M. M. (2017). "Quantifying streambank movement and topography using unmanned aircraft system photogrammetry with comparison to terrestrial laser scanning." *River Research and Applications*, 33(8), 1354–1367.

Hamshaw, S. D., Engel, T., O'Neil-Dunne, J., Rizzo, D. M., and Dewoolkar, M. M. (2018). "Application of unmanned aircraft system (UAS) for monitoring bank erosion along river corridors." *Geomatics, Natural Hazards and Risk*, In Press.

Ishee, E. R., Ross, D. S., Garvey, K. M., Bourgault, R. R., and Ford, C. R. (2015). "Phosphorus Characterization and Contribution from Eroding Streambank Soils of Vermont's Lake

Champlain Basin." *Journal of Environment Quality*, 44(6), 1745.
James, M. R., Robson, S., and Smith, M. W. (2017). "3-D uncertainty-based topographic change detection with structure-from-motion photogrammetry: precision maps for ground control and directly georeferenced surveys." *Earth Surface Processes and Landforms*.
Keane, T. D., and Sass, C. K. (2017). "Channel Evolution Models as Predictors of Sediment Yield." *JAWRA Journal of the American Water Resources Association*, 53(6), 1513–1529.
Kline, M., and Cahoon, B. (2010). "Protecting River Corridors in Vermont1." *JAWRA Journal of the American Water Resources Association*, 46(2), 227–236.
Lawler, D. M. (1993). "The measurement of river bank erosion and lateral channel change: A review." *Earth Surface Processes and Landforms*, 18(9), 777–821.
Michalková, M., Piégay, H., Kondolf, G. M., and Greco, S. E. (2011). "Lateral erosion of the Sacramento River, California (1942–1999), and responses of channel and floodplain lake to human influences." *Earth Surface Processes and Landforms*, 36(2), 257–272.
Milan, D. J., Heritage, G. L., and Hetherington, D. (2007). "Application of a 3D laser scanner in the assessment of erosion and deposition volumes and channel change in a proglacial river." *Earth Surface Processes and Landforms*, 32(11), 1657–1674.
Miřijovský, J., and Langhammer, J. (2015). "Multitemporal Monitoring of the Morphodynamics of a Mid-Mountain Stream Using UAS Photogrammetry." *Remote Sensing*, 7(7), 8586–8609.
Olson, S. A. (2014), Estimation of flood discharges at selected annual exceedance probabilities for unregulated, rural streams in Vermont, *with a section on* Vermont regional skew regression, by Veilleux, A. G., *Scientific Investigations Report 2014–5078*, U.S. Geological Survey, Washington, D. C.
Ross, D. S., Wemple, B. C., Willson, L. J., Balling, C., Underwood, K. L., and Hamshaw, S. D. (2018). "Impact of an Extreme Storm Event on River Corridor Bank Erosion and Phosphorus Mobilization in a Mountainous Watershed in the Northeastern USA." *Journal of Geophysical Research: Biogeosciences*, Revision in Review.
Springston, G, E. Thomas and J. Kim (2014), Surficial Geologic Map of the northern 2/3 of the South Mountain Quadrangle, Vermont: VGS Open File Report VG14-2, Vermont Geological Survey, Montpelier, VT.
Tamminga, A. D., Hugenholtz, C., Eaton, B., and Lapointe, M. (2015). "Hyperspatial Remote Sensing of Channel Reach Morphology and Hydraulic Fish Habitat Using an Unmanned Aerial Vehicle (UAV): A First Assessment in the Context of River Research and Management." *River Research and Applications*, 31(3), 379–391.
Thoma, D. P., Gupta, S. C., Bauer, M. E., and Kirchoff, C. E. (2005). "Airborne laser scanning for riverbank erosion assessment." *Remote Sensing of Environment*, 95(4), 493–501.
Underwood, K. L. (2004). *Phase 2 Stream Geomorphic Assessment New Haven River Watershed Addison County, Vermont*. Addison County Regional Planning Commission, Middlebury, Vermont.
Underwood, K. L., Libby, S., Pytlik, S., Jaquith, S., Smith, C., & McKinley, D., (2014). A Conservation Partnership to Restore Ecosystem Services along the New Haven River. *38th Annual New England Association of Environmental Biologists conference*, Burlington, VT
United States Department of Agriculture (USDA), Natural Resources Conservation Service, Soil Survey Staff. Soil Survey Geographic (SSURGO) Database for Addison County, VT. Available online. Accessed 6/5/2018. http://maps.vcgi.vermont.gov/gisdata/vcgi/packaged_zips/GeologicSoils_SO/
Winterbottom, S. J., and Gilvear, D. J. (2000). "A GIS-based approach to mapping probabilities

of river bank erosion: regulated River Tummel, Scotland." *Regulated Rivers: Research & Management*, 16(2), 127–140.

Wohl, E., Lane, S. N., and Wilcox, A. C. (2015). "The science and practice of river restoration." *Water Resources Research*, 51(8), 5974–5997.

Woodget, A. S., Carbonneau, P. E., Visser, F., and Maddock, I. P. (2015). "Quantifying submerged fluvial topography using hyperspatial resolution UAS imagery and structure from motion photogrammetry." *Earth Surface Processes and Landforms*, 40(1), 47–64.

Reliability-Based Stability Analysis of Fiber-Reinforced Infinite Slopes

Assile Abou Diab[1]; Shadi Najjar, A.M.ASCE[2]; and Salah Sadek, M.ASCE[3]

[1]Assistant Professor, College of Architectural Engineering and Digital Design, Dar Al Uloom Univ., Riyadh, KSA. E-mail: assil@dau.edu.sa
[2]Associate Professor, Dept. of Civil and Environmental Engineering, American Univ. of Beirut, PO Box 11-0236, Riad El-Solh 1107-2020. E-mail: sn06@aub.edu.lb
[3]Professor, Dept. of Civil and Environmental Engineering, American Univ. of Beirut, PO Box 11-0236, Riad El-Solh 1107-2020. E-mail: salah@aub.edu.lb

ABSTRACT

Fiber-reinforcement has been proven to be an effective technique for stabilizing new or existing slopes against shallow failures. For sandy soil, the main benefit of fiber reinforcement is the increase in the friction angle. Such an increase will theoretically allow for designing slopes that are steeper or higher for any given design factor of safety. The friction angle of fiber-reinforced sand can be predicted from the properties of the unreinforced sand and the properties of the individual fibers using available discrete or energy-based empirical models. It has been proven that these model predictions suffer from a given level of model uncertainty. As a result, the predicted friction angle of fiber-reinforced sand may be more uncertain than that of unreinforced sand. In this study, the uncertainty in the friction angle of fiber-reinforced sand is quantified by combining traditional spatial variability with model uncertainty. The combined uncertainty is then incorporated in a reliability-based design methodology that is tailored for assessing the risk of failure of fiber-reinforced infinite slopes. The results indicate that the design factor of safety against slope stability failure may have to be increased in fiber-reinforced infinite slopes to maintain the same level of reliability as traditional non-reinforced slopes. The required factor of safety is affected by the choice of the model used to predict the fiber-reinforced friction angle and by the anticipated degree of spatial variability in the friction angle of the unreinforced soil.

INTRODUCTION

The safety of sandy slopes against shallow failures is usually evaluated using the infinite slope theory (Wright and Duncan, 2005). The inclusion of discrete fibers is reported to increase the friction angle of sand (Maher and Gray, 1990; Consoli et al., 2005; Sadek et al., 2010; among others). As such, fiber reinforcement is deemed to be a viable soil improvement technique that allows the design of steeper slopes for any given design factor of safety (FS). Alternatively, if the slope angle is to be maintained constant, fiber reinforcement will increase the safety factor of the slope, which is ideal for the repair of slopes that have already failed at their current slope angle.

From a practical design standpoint, the safety of an infinite slope is assessed based on a deterministic factor of safety which is expected to implicitly cover all the uncertainties in the input parameters and the model error. However, it has been shown that slopes designed for the same deterministic FS may entail different probabilities of failure/levels of risk. For fiber-reinforced slopes, the problem is amplified by the additional source of uncertainty resulting from the models used to predict the friction angle of the reinforced soil. A reliability-based framework can be utilized to systematically combine the uncertainties in soil parameters, spatial variability, and model errors for the purpose of assessing the probability of failure of infinite slopes designed with fiber-reinforced sands. A thorough review of the literature shows that the published studies on the reliability of infinite slopes only consider unreinforced sand cases (Griffiths et al., 2011; Li et al., 2014; Cai et al., 2017) while no attention is given to slopes involving fiber-reinforced sands.

This paper presents a reliability-based procedure that utilizes the Monte-Carlo simulation technique and random field theory to assess the reliability of fiber-reinforced sand infinite slopes. Uncertainty in the unreinforced friction angle (ϕ'_{unr}) is represented by a random field that is characterized by a mean, coefficient of variation, and a vertical scale of fluctuation. In the Monte Carlo simulations, values of unreinforced friction angle are generated from the random field and combined with assumed fiber properties to evaluate the corresponding values of the reinforced friction angle. The uncertainty in the predictions of fiber-reinforced sand models as quantified in Najjar et al. (2013) is then incorporated in the analysis to evaluate the total uncertainty in the reinforced friction angle (ϕ'_R) which is then used to assess the probability of failure of a given slope design. Najjar et al. (2013) evaluated the model uncertainty of the “energy-based” and “discrete” models that are used to estimate the strength of fiber-reinforced sands and introduced minor modifications to these models to improve their predictive capacity. In addition to the friction angle which was treated as a random field, the unit weight and pore water pressure were treated as random variables. In this study, it was assumed that the theoretical formulation of infinite slopes has no model error and that the slope angle is deterministic.

INFINITE SLOPE THEORY

An infinite slope analysis is rigorous and valid for sandy slopes where it is possible for a slip surface to form at a small enough depth (Duncan and Wright, 2005). In the deterministic analysis, the slope is assumed to be homogeneous and is characterized by the average values of soil properties. The FS in this case is expressed as:

$$\mathrm{FS} = \left[\cot\theta - \frac{\mathrm{u}}{\gamma \mathrm{H}}\left(\cot\theta + \tan\theta\right)\right]\tan\phi'_{unr} \tag{1}$$

where u is the pore water pressure at the depth H of the slip surface, γ and ϕ'_{unr} are respectively the total unit weight and the effective friction angle of the sand, and θ is the slope angle.

For seepage parallel to the slope, u is given by:

$$\mathrm{u} = \gamma_w h_w \cos^2\theta \tag{2}$$

where γ_w and h_w are the unit weight of the water and the height of water above the slip surface, respectively. The configuration of the fiber-reinforced sandy infinite slope is shown in Figure 1 for the case of seepage parallel to the slope.

UNCERTAINTY IN SOIL PROPERTIES AND IN PREDICTIONS OF FRICTION ANGLE OF FIBER-REINFORCED SAND

In the reliability analysis, the friction angle of the unreinforced sand, the bias factor of the predictive models of the friction angle of fiber-reinforced sand (defined in this paper as the ratio of the predicted friction coefficient ($(\tan \phi'_R)_{pred}$) to the measured friction coefficient ($(\tan \phi'_R)_{meas}$)), the unit weight of the reinforced sand, and the height of water above the slip surface are treated as random fields/variables defined by a distribution, a mean, and a coefficient of variation (COV), as shown in Table 1 (Lacasse and Nadim,1996; Griffiths et al., 2011). For simplicity, the maximum depth to the potential failure surface (H), the slope angle, and the properties of the fibers are considered deterministic in this study.

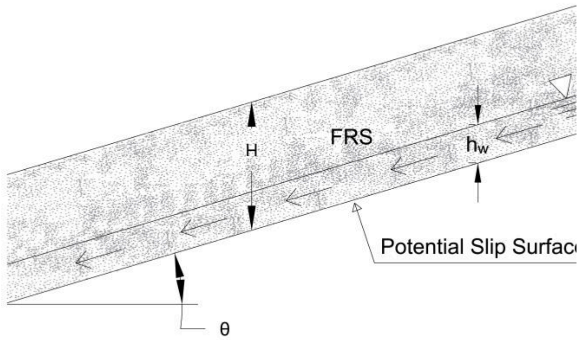

Figure 1. Fiber-reinforced infinite slope with seepage parallel to slope.

Table1: Parameters used in the simulations

Random Variable	Distribution	Mean	COV
ϕ'_{unr}(°)	Truncated Normal	33	0.05, 0.10, 0.15
$\lambda_{Zornberg}$	Lognormal	1.06	0.17
$\lambda_{Zornberg,modified}$	Lognormal	1	0.12
$\lambda_{Michalowski}$	Normal	0.9	0.20
$\lambda_{Michalowski,modified}$	Normal	1.02	0.17
h_w (m)	Lognormal	1.5	0.1
γ (KN/m^3)	Lognormal	17	0.03

Although many studies in the field of probabilistic infinite slope analysis have considered unbounded lognormal distributions for the angle of friction of sand (Griffiths et al. 2011, Li et al. 2014), the values of ϕ'_{unr} in this study are constrained to a lower limit of 25° and an upper limit of 55° (Ching et al. 2012) in order to restrict the simulations to realistic limits and avoid the generation of occasional extreme values. The models proposed by Zornberg (2002) and Michalowski and Cermark (2003) in addition to the modified versions of these models (Najjar et al. 2013) were used to predict the friction angle of fiber-reinforced sand.

In the discrete model developed by Zornberg (2002), the equivalent shear strength of purely frictional soil is given by:

$$\tan\phi'_R = \left(1+\alpha.\eta_F.\chi_F.c_{i,\varphi}\right)\cdot\tan\phi'_{unr} \tag{3}$$

where α = empirical coefficient that accounts for the orientation of fibers (assumed to be equal to 1), η_F = fiber aspect ratio defined as ratio of the length of the fiber to its diameter, χ_F = volumetric fiber content, $c_{i,\varphi}$ interaction coefficient for the frictional component of the interface shear strength (assumed to be equal to 0.8. Li and Zornberg, 2003).

Michalowski and Cermak (2003) proposed an energy dissipation model where the improved equivalent internal friction angle is given by:

$$\phi'_R = 2\cdot\tan^{-1}\sqrt{\frac{\eta_F\cdot\chi_F\cdot M\cdot c_{i,\varphi}\cdot\tan\varphi'_{unr}+6\cdot\tan^2\left(45°+\varphi'_{unr}/2\right)}{6-\eta_F\cdot\chi_F\cdot M\cdot c_{i,\varphi}\cdot\tan\varphi'_{unr}}}-\frac{\pi}{2} \tag{4}$$